Numerical simulation of turbulent two-phase flows

S. Neti and O. E. E. Mohamed
Department of Mechanical Engineering and Mechanics, Lehigh University, Bethlehem, PA, USA

A two-equation turbulent model for steady incompressible two-phase flows was developed to predict multiphase flow phenomenon from the Navier–Stokes equations. Turbulent two-phase bubbly noncondensing jet flows and pipe flows were investigated. The numerical computations used an Eulerian system to describe the continuous (liquid) phase and a Lagrangian approach for simulating the effects of the dispersed (gaseous) phase. Source terms were used to couple the two approaches. A deterministic separated flow model was used to predict the bubbly jets, whereas a stochastic separated flow model was developed to describe the bubbly flow in vertical pipes. The deterministic model allows for bubble interactions with the liquid mean properties, whereas the stochastic model takes into account the instantaneous transport properties of the bubbles and the liquid.

The addition of even small amounts of air increases flow turbulence levels noticeably. At higher void fractions, the effects of the second phase were large, justifying the need for a detailed model of the energy production and dissipation mechanisms to predict the two-phase flow. These effects were included in the k–ε model of turbulence used here and required introduction of two additional constants for closure. The additional constants were evaluated using the limited experimental data available. The model's two-phase flow computations yielded very good predictions of flow details. Predictions of the radial distributions of mean velocity and turbulence intensity compared well with the experimental data available in the literature.

Keywords: two-phase; numerical simulation; turbulence; k–ε model; pipe flow; jet flow

Introduction

Two-phase flows occur in an extremely wide range of environmental situations and industrial plants, including nuclear reactors and conventional power generating plants, as well as in air-conditioning and refrigeration equipment. Industrial applications have generated substantial interest in formulation and modeling of two-phase flow systems. This interest is reflected in the voluminous literature in this field. Understanding two-phase flows is difficult, because the properties of both phases are influenced by transport within a generally turbulent environment. Furthermore, bubbly flows of interest here are not particularly amenable to empirical correlations. Their structure is influenced by the geometry and size of the system, size distribution of the bubbles, media of each phase, effects of initial conditions and buoyancy, energy exchanged between phases, and relevant interphase transport processes, such as whether the bubbles are condensing, changing in size, etc. Owing to these complexities, fundamental understanding of bubbly two-phase systems is still lacking. Our investigation concentrated on steady, low-void fraction, axisymmetric, turbulent, bubbly flows in vertical, round jets and circular tubes.

The two-phase bubbly jets consist of air bubbles and water being injected vertically upward in a rectangular tank filled with water. For the vertical circular tubes, air bubbles are injected into the tube through which water is flowing upward or downward. Sufficiently high Reynolds numbers are assumed, and the flow is considered axisymmetric and turbulent. Local properties of the gaseous and liquid phases are not assumed to be the same; e.g., there is a velocity difference (slip) between the phases, and similar differences persist with respect to the turbulence intensities of the two phases. Buoyancy forces can be very important, tending preferentially to accelerate the bubbles in the upward flow.

With these assumptions, the problem associated with simulating detailed flow patterns involves the solution of strongly coupled, nonlinear partial differential equations for the conservation of mass and momentum and lies well beyond any foreseeable analytical approach. Hence we used a numerical approximation, along with the Prandtl–Kolmogorov effective viscosity hypothesis for the continuous phase (turbulence model) to avoid an impractically large number of calculations. We utilized a stochastic Lagrangian (bubble-tracking) method to complete the picture of the gas–liquid bubbly phenomenon.

Literature review

The bubbly flow pattern is characterized by a suspension of discrete bubbles in a continuous liquid and is one of the flow regimes in which lateral mixing is significant. For this and other reasons, the lateral phase-distribution mechanism is one of the most important, yet least understood, aspects of two-phase flow.

The basic laws used to predict the hydrodynamic and thermodynamic behavior of two-phase flow are the same as those that govern single-phase flow. However, describing the two-phase phenomenon requires at least twice as many basic equations as the single-phase case. Generally, two-phase flow problems are represented mathematically using the Eulerian method of fluid mechanics, treating each phase as a continuum,

Address reprint requests to Dr. Neti at the Department of Mechanical Engineering and Mechanics, Lehigh University, Bethlehem, PA 18015, USA.

Received 25 August 1989; accepted 15 January 1990

over a control volume with the interfacial interactions described by the so-called constitutive relations. Considerable uncertainty about two-phase flows remains, even in the formation of these constitutive relations. In addition, the turbulent fluctuation terms that appear in the original governing equations are ignored or claims are made that they are included in the interphase exchange equations. Most two-phase flows of interest are highly turbulent, the phase interaction models must account for the role of turbulence, and thus the terms containing the temporal and spatial fluctuations in the conservation equations must be recognized.

Various mathematical models for two-phase flows have been developed, including those by Ishii and Mishima,[1] Sun *et al.*,[2–5], Schor *et al.*,[6] and Spore *et al.*[7] Sun *et al.*[2–5] studied the structure of turbulence in condensing and noncondensing, bubbly, upward-flow jets. Their studies show that stochastic separated flow analysis yields better predictions than do locally homogeneous flow models or deterministic separated flow models. In the deterministic models, interphase transport rates are assumed to be finite and the dispersed phase is assumed to interact only with the mean properties of the continuous phase. The stochastic analysis uses finite interphase transport rates, and the effects of turbulence on the dispersed phase are treated using random-walk calculations, requiring much more formulational effort and computer time.

Two-phase bubbly flows have received considerable experimental attention, as summarized in a review of Abdel-Aal *et al.*[8] Goldschmidt *et al.*[9] measured turbulence properties in very dilute bubbly jets (maximum void fraction of 0.4%) and suggested that, even at these conditions, continuous-phase turbulence properties are modified by bubbles. Chesters *et al.*[10] used laser-Doppler anemometry (LDA) and a double-electrode probe to measure mean liquid and bubble velocities in bubbly plumes. Sun[5] and Sun *et al.*[2–4] used LDA to measure mean and fluctuating phase velocities and the Reynolds stress of the liquid phase. They also measured the distribution of bubbles and bubble sizes, using flash photography. Three different cases, distinguished by the void fraction (all less than 10%), have been investigated.[5,11]

Many other investigators have studied gas–liquid mixture bubbly flows, both experimentally and theoretically, e.g., Theofanous and Sullivan,[12] Serizawa *et al.*,[14–16] Neti and Colella,[17] Marie,[18] and Lance and Bataille.[19] However, some inconsistencies among the data from different sources remain unresolved, probably because of inadequate two-phase flow constitutive models and insufficient basic two-phase flow data. For example, the earlier data of Serizawa indicate that turbulence intensity is not strongly affected by the amount of gas flow, whereas Theofanous and Sullivan's and Neti and Colella's data imply otherwise. Although Neti and Theofanous agreed that turbulence intensities increased with quality (mass fraction of gases), comparison of their results does not completely support this conclusion. Neti ascribes this discrepancy to the different bubble sizes used in the two experiments. Possibly in support of this conclusion, Lance and Bataille[19] recently reported the strong dependence of turbulent intensities on void fraction and bubble size.

As we mentioned earlier, the lateral phase-distribution mech-

Notation

a, b	Coefficients in the discretized equations
C_D	Drag coefficient
C_1, C_2	Empirical constants in the k–ε model
C_3, C_k	Empirical constants in the k–ε model
C_μ	Constant in the k–ε model of turbulence, 0.09
d	Injector diameter
d_p	Bubble diameter
D	Pipe diameter
E	Constant in the law of the wall
F_e	Body force
g	Acceleration of gravity
k	Turbulence kinetic energy
l	Mixing length
m_p	Bubble mass flow rate
P	Pressure
Pe	Peclet number, $\rho u \delta/\Gamma$
r	Radial distance, y direction
R	Radius of the pipe
Re	Reynolds number, $(UD)/\nu$
Re_p	Bubble Reynolds number, $(U_p - U)d_p/\nu$
s	Dummy variable
S	Source term
t	Time
t_p	Time of particle motion
u	Instantaneous velocity component, x direction
u'	Fluctuating part of velocity component, x direction
U	Mean part of velocity component, x direction
v	Instantaneous velocity component, r direction
v'	Fluctuating part of velocity component, r direction
V	Mean part of velocity component, r direction
x, y	Coordinate directions: x = axial direction; y = radial direction (r)

Greek symbols

α	Void fraction
β_i	Fraction of bubble mass that enters at port i
Γ_Φ	General diffusion coefficient
δ	Distance between grid nodes
δ_{ij}	Kronecker's delta function
Δ_A	Correction for virtual mass force, 2.1
Δ_H	Correction for Basset history force, 0.48
ΔV	Volume corresponding to a control volume
Δt	Time over which source terms or bubble transit are calculated
ε	Dissipation rate of turbulence energy
κ	von Karman constant
μ	Molecular viscosity
ν	Dynamic viscosity, μ/ρ
ν_t	Eddy diffusivity
ρ	Density
$\rho\overline{u'_j u'_j}$	Reynolds stress
σ_k	Constant in the k–ε model
σ_ε	Constant in the k–ε model
τ_e	Life of an eddy
τ_w	Wall shear stress
Φ	General variable, transported scalar

Subscripts

c	Centerline
e, E	East
eff	Effective
ε	Index to ε equation
k	Index to k equation
i, j	Summation indices in tensor notation
t	Turbulent
u	Index to x direction momentum
v	Index to r direction momentum

anism is one of the most important aspects of two-phase flows. The lateral void fraction distribution for a bubbly flow apparently was first analyzed by Bankoff.[20] He assumed a power law distribution for both the velocity and the void fraction, with the maximum void fraction at the centerline of the pipe, decreasing monotonically in the radial direction and vanishing at the pipe wall. Levy[21] and Beattie[22] used mixing-length models to predict velocity distribution and void fraction profiles, respectively, both of which peaked at the centerline. Yet, experiments by Serizawa *et al.*,[15] Sekoguchi *et al.*,[23] Wang *et al.*,[24] and Spindler *et al.*[25] have shown that, in some cases, the highest void concentration in upward cocurrent flow exists close to the wall of the flow section. Influence of entrance effects on void distribution may also be important, as suggested by Spindler *et al.*[25] and Herringe *et al.*[26,27]

In summary, the structure of two-phase bubbly pipe flows is still not that well understood. Moreover, some new experimental findings for these flows (e.g., newly measured radial void fraction distribution) seem to vary from earlier published data. A complete model from fundamental Navier–Stokes equations, for turbulent two-phase bubbly flows, that fully describes the effects of dispersed-phase (bubbles) on continuous-phase (liquid) turbulence does not exist. Although such a basic tool for prediction of this important phenomenon would be welcome, numerical predictions are likely to remain the best means of explaining it for now. In this work we present numerical solutions of the two-phase transport equations that include the effect of the dispersed phase on the continuum in an attempt to better understand these flows from first principles.

Model equations and solution procedure

The two phases of gas–liquid bubbly flows are modeled to highlight the important features of their transport properties. In such flows, the continuous (liquid) phase is most conveniently described by an Eulerian system, whereas the dispersed (gaseous) phase is more amenable to a Lagrangian description, particularly at low concentrations of the dispersed phase. We treat the interfacial exchanges by means of the physically appealing and computationally convenient concept of source terms.

The equations for the continuous phase are those that describe axisymmetric, incompressible, steady, turbulent flows. They are presented in the Reynolds averaged form using the Boussinesq hypothesis for the Reynolds stresses ($\overline{u'u'}$, $\overline{u'v'}$, and $\overline{v'v'}$).

- *Continuity:*

$$\frac{\partial}{\partial x}(r\rho U)+\frac{\partial}{\partial r}(r\rho V)=0 \tag{1}$$

- *U momentum:*

$$\frac{\partial}{\partial x}(\rho U^2)-\frac{\partial}{\partial x}\left(\mu_{\text{eff}}\frac{\partial U}{\partial x}\right)+\frac{1}{r}\frac{\partial}{\partial r}(r\rho UV) -\frac{1}{r}\frac{\partial}{\partial r}\left(r\mu_{\text{eff}}\frac{\partial U}{\partial r}\right)=S_U+S_{pU} \tag{2}$$

- *V momentum:*

$$\frac{\partial}{\partial x}(\rho UV)-\frac{\partial}{\partial x}\left(\mu_{\text{eff}}\frac{\partial V}{\partial x}\right)+\frac{1}{r}\frac{\partial}{\partial r}(r\rho V^2) -\frac{1}{r}\frac{\partial}{\partial r}\left(r\mu_{\text{eff}}\frac{\partial V}{\partial r}\right)=S_V+S_{pV} \tag{3}$$

As described elsewhere,[28,29] the source terms S_U, S_{pU}, S_V, and S_{pV} include all other relevant terms in the momentum equations. For example, in the U-momentum equation, the pressure-drop term $(-\partial P/\partial x)$ would be part of S_U, and any linearized contributions that are functions of U would be included in S_{pU}. In addition, these source terms also account for the effect of the second phase or other phenomenon. We present details pertaining to the influence of the second phase, both in the context of mean properties and with respect to turbulence. The effective viscosity, μ_{eff}, includes the turbulence contributions and is calculated using a two equation (k–ε) turbulence model[30] and is described later.

Evaluation of the contributions of bubbles requires characterization of bubble trajectory histories. We do so by integrating the bubble equations of motion. The general form of this equation, for spherical bubbles when the bubble movements are within the Stokes regime (low Reynolds numbers, Re_p based on relative velocity and bubble diameter), is[26,31,32]

$$\frac{\pi}{6}d_p^3\rho_p\frac{du_{pi}}{dt_p}=\frac{\pi}{8}d_p^2\rho C_D|u_{ri}|(u_i-u_{pi})-\frac{\pi}{6}d_p^3\frac{\partial P}{\partial x_i}-\frac{\pi}{12}d_p^3\rho\frac{du_{ri}}{dt_p} +\tfrac{3}{2}d_p^2(\pi\rho\mu)^{1/2}\int_{t_0}^{t}(t-s)^{-1/2}\frac{d(u_i-u_{pi})}{ds}\,ds+F_e \tag{4}$$

where d_p is the bubble diameter, ρ_p is the dispersed-phase (gas) density, u_{pi} is the bubble velocity in the i direction, t_p is the initial time for the bubble motion, ρ is the continuous-phase (liquid) density, C_D is the drag coefficient, $|u_{ri}|$ is the magnitude of the relative velocity vector, u_i is the continuous-phase velocity in the i direction, P is the pressure, x_i is the coordinate in the i direction, μ is the continuous-phase molecular viscosity, t is time, and s is a dummy variable. The time derivative is taken following the motion of the bubble:

$$\frac{d}{dt_p}=\frac{\partial}{\partial t}+u_{pi}\frac{\partial}{\partial x_i} \tag{5}$$

The term on the left-hand side of Equation 4 represents the inertia of the sphere. Taken in order, the terms on the right-hand side of Equation 4 represent the drag force on the sphere, including skin friction and form drag; the force on the sphere from the static pressure gradient in the flow; the force on the sphere from the inertia of the fluid displaced by its motion, often called the *virtual mass term*; the Basset term, which allows for the effects of the deviation of the flow from a steady flow pattern around the sphere; and the external body force term.

When all external forces except the drag, virtual mass, buoyancy, and Bassett forces are neglected with $\rho/\rho_p\simeq 10^3$, the equation of motion extended empirically to Reynolds numbers beyond the Stokes regime (Clift *et al.*[33]) can be expressed as

$$\frac{\Delta_A}{2}\frac{du_{ri}}{dt}=g\delta_{1i}-\frac{3C_D}{4d_p}|u_r|u_{ri}-\Delta_H\left(\frac{81\nu}{\pi d_p^2}\right)^{1/2}\int_{t_0}^{t}(t-s)^{-1/2}\frac{du_{ri}}{ds}\,ds \tag{6}$$

where u_{ri} is the difference between bubble and liquid velocities ($i=1$ or 2; u_{r1} axial and u_{r2} radial velocity), Δ_A is a correction for the virtual mass term ($\simeq 2.1$), δ_{ij} is the Kronecker delta function (with $j=1$ for liquid and 2 for bubbles), g is gravitational acceleration, Δ_H is a correction for the Basset history force ($\simeq 0.48$), and ν is the liquid kinematic viscosity.

Equation 6 is supplemented by the trajectory equations, giving the rate of change of location with respect to time:

$$\frac{dx_p}{dt}=u_p \quad \text{and} \quad \frac{dy_p}{dt}=v_p \tag{7a,b}$$

where x_p and y_p are the axial and radial bubble coordinates at time t. The drag coefficient depends on the bubble Reynolds

number (Re_p)—based on the gas–liquid relative velocity—and is evaluated per Clift *et al.*[33] and Peebles and Garber.[34]

We can decompose the instantaneous bubble velocities u_p and v_p, using Reynolds averaging, as $u_p = U_p + u'_p$ and $v_p = V_p + v'_p$. We adopted a stochastic approach[5,35] for evaluation of the instantaneous fluctuating velocity components that appear in the equation of bubble motion. We sampled the values of u' and v' that prevail during the life of a liquid eddy the bubble is traversing by assuming that they possess a Gaussian probability distribution. Hence

$$u' = \gamma(\overline{u'^2})^{1/2} \quad \text{and} \quad v' = \gamma(\overline{v'^2})^{1/2} \tag{8a,b}$$

where γ is a normally distributed random variable, $(\overline{u'^2})^{1/2}$ and $(\overline{v'^2})^{1/2}$ are the rms values of the fluctuations at the point where the bubble is engulfed by a particular group of eddies having the same properties. The magnitudes of u' and v' remain unchanged[5,35] so long as the life of the eddy is less than

$$\tau_e = \frac{C_\mu^{3/4} k^{3/2}}{\varepsilon(\overline{u'^2} + \overline{v'^2})^{1/2}} \tag{9}$$

We obtain the bubble trajectories by solving Equations 6 and 7, using the Runge–Kutta method.

The entry of bubbles into two-phase flow is represented by a finite number of entry ports (NPL). The mass of bubbles of size, d_{pj}, that enter per unit time at port i is

$$m_{pi}(d_{pj}) = m_p \beta_i \omega_j \tag{10}$$

where m_p is the total bubble mass inflow rate, β_i is the fraction of the bubble mass that enters at port i, and ω_j is the fraction of the bubble mass with initial diameter d_{pj}. The number of bubbles of initial diameter d_{pj} flowing out of a given port is

$$n_i(d_{pj}) = \frac{6 m_p \beta_i \omega_j}{\pi \rho_p d_{pj}^3} \tag{11}$$

if we assume that the bubbles are spherical and ρ_p is the density of the bubble fluid. The number of these bubbles $n_i(d_{pj})$ from a specific port remains constant, because no bubble shattering or coalescence is allowed. Owing to computer limitations, only a fraction of these $n_i(d_{pj})$ bubbles are simulated to get stochastic information. Overall bubble effects are calculated on the basis of this fraction of the total bubbles simulated.

As mentioned earlier, the source terms S_{pU} and S_{pV} include contributions to the liquid momentum equations by bubble motion. We evaluate S_{pU} and S_{pV} on a per unit volume basis by considering the sum of contributions over a control volume. Of interest here is the net flux rate of liquid momentum caused by bubbles of size d_{pj}, which enter the flow at port i and are calculated as follows:[36]

$$S_{pU} = S_p U + S_{uu} \tag{12}$$

$$S_{pV} = S_p V + S_{uv} \tag{13}$$

where

$$S_p = -\frac{1}{\Delta V} \sum_{i=1}^{\text{NPL}} \sum_{j=1}^{\text{NPS}} \sum_{k=1}^{\text{NPG}} [m_{pi}(d_{pj}) f \Delta t]_k \tag{14}$$

$$S_{uu} = \frac{1}{\Delta V} \sum_{i=1}^{\text{NPL}} \sum_{j=1}^{\text{NPS}} \sum_{k=1}^{\text{NPG}} \left\{ m_{pi}(d_{pj}) \left[f u_{p,\text{out}} \Delta t - \frac{\rho}{\rho_p} (u_{p,\text{in}} - u_{p,\text{out}}) \right] \right\}_k \tag{15}$$

$$S_{uv} = \frac{1}{\Delta V} \sum_{i=1}^{\text{NPL}} \sum_{j=1}^{\text{NPS}} \sum_{k=1}^{\text{NPG}} \left\{ m_{pi}(d_{pj}) \left[f v_{p,\text{out}} \Delta t - \frac{\rho}{\rho_p} (v_{p,\text{in}} - v_{p,\text{out}}) \right] \right\}_k \tag{16}$$

where

NPS is the number of bubble sizes (5);

NPL is the number of bubble entry ports (7);

NPG is the number of bubbles of a certain diameter from one entry port ($\simeq$1–20);

$f = \dfrac{C_D \mathrm{Re}_p}{24} \dfrac{18_\mu}{d_{pj}^2 \rho_p}$; and

$\dfrac{d_{pj}^2 \rho_p}{18\mu}$ is the response time of a bubble of size d_{pj}.

For the bubble entry port (i=1 to NPL) chosen for calculation and based on β_i, the fraction of bubble mass entering at entry port i, and ω_j, the assumed fraction of bubble mass with initial diameter d_{pj}—and knowing the total number of bubbles to be studied—we "introduce" a desired bubble into the liquid flow. The total number of bubbles of a diameter from one such entry port (NPG) varied from 1 to 20. Bubble trajectory is determined from Equations 7 and 8. As bubble trajectories are determined, bubble contributions to the local control volume that they pass through are evaluated with Equations 14–17. That is, after the bubble paths and source terms for the fraction of total $n_i(d_{pj})$ bubbles used have been analyzed one by one, they are added. The resulting sums S_{pU} and S_{pV} represent the contributions to be added to the liquid momentum equations, Equations 2 and 3.

In our k–ε model, we use transport equations to determine turbulent kinetic energy and dissipation rate distributions.

- *k equation:*

$$\frac{\partial}{\partial x}(\rho U k) + \frac{1}{r}\frac{\partial}{\partial r}(r \rho V k) - \frac{\partial}{\partial x}\left(\frac{\mu_{\text{eff}}}{\sigma_k}\frac{\partial k}{\partial x}\right) - \frac{1}{r}\frac{\partial}{\partial r}\left(r \frac{\mu_{\text{eff}}}{\sigma_k}\frac{\partial k}{\partial r}\right) = S_k + S_{pk} \tag{17}$$

- *ε equation:*

$$\frac{\partial}{\partial x}(\rho U \varepsilon) + \frac{1}{r}\frac{\partial}{\partial r}(r \rho V \varepsilon) - \frac{\partial}{\partial x}\left(\frac{\mu_{\text{eff}}}{\sigma_\varepsilon}\frac{\partial \varepsilon}{\partial x}\right) - \frac{1}{r}\frac{\partial}{\partial r}\left(r \frac{\mu_{\text{eff}}}{\sigma_\varepsilon}\frac{\partial \varepsilon}{\partial r}\right) = S_\varepsilon + S_{p\varepsilon} \tag{18}$$

where

$$S_k = G - \rho\varepsilon \qquad S\varepsilon = \frac{C_1 G \varepsilon}{k} - \frac{C_2 \rho \varepsilon^2}{k}$$

$$G = \mu_{\text{eff}} \left\{ 2 \left[\left(\frac{\partial U}{\partial x}\right)^2 + \left(\frac{\partial V}{\partial r}\right)^2 + \left(\frac{\partial U}{\partial x} + \frac{\partial U}{\partial x}\right)^2 + \frac{V}{r^2} \right] \right\}$$

and S_{pk} and $S_{p\varepsilon}$ are source terms representing the contributions by the bubbles to the appropriate equation. We evaluate normal stresses $\overline{u'^2}$ and $\overline{v'^2}$ in two-phase pipe flow from k, assuming that $\overline{u'^2}:\overline{v'^2} = k:k/2$, which is the ratio observed near the axis,[24] although the axial normal stress is more dominant close to the wall. The constants in the k–ε model are essentially the same as those used for single-phase flows, except for the special treatment of C_1 and κ described later. The constants used are $C_\mu = 0.09$, $\sigma_k = 1.0$, $C_2 = 1.87$, and $\sigma_\varepsilon = 1.3$ for jetflows; and $C_2 = 1.92$ and

$$\sigma_\varepsilon = \frac{\kappa^2}{(C_2 - C_1) C_\mu^{1/2}}$$

for pipe flows.

Introduction of the gaseous phase into the flow increases the friction factor because of the production of turbulence energy by bubbles. The mixing length relation, $l = \kappa y$, is modified to

account for the presence of the gaseous phase[31] as

$$\kappa_{TP}=\Phi_{LO}^2\kappa \tag{19}$$

and the constant, C_1, in the ε equation, consequently, is modified to be

$$C_1=C_2-\frac{\kappa_{TP}^2}{\sigma_\varepsilon C_\mu^{1/2}} \tag{20}$$

where the subscript TP represents two-phase quantity, κ is Karman's constant (0.4187), and Φ_{LO}^2 is a two-phase multiplier[32] given in terms of the quality (mass fraction of gaseous phase x_v), of the flow

$$\Phi_{LO}^2=\left[1-x_v\left(\frac{\rho}{\rho_p}-1\right)\right] \tag{21}$$

The effects of bubble source terms in the governing equations for turbulence quantities were investigated by Al-Taweel and Landau.[37] In considering these terms, we followed the approach of Shuen *et al.*[35,38] and Parthasarathy and Faethn[39]:

$$S_{pk}=\overline{S_{pu}u}-\overline{S_{pu}}\,\overline{u} \tag{22}$$

where S_{pk} is the source term in the k equation owing to the bubbles, and $S_{p\varepsilon}$, the source term in the ε equation, is related to S_{pk} by

$$S_{p\varepsilon}=-C_3\frac{S_{pk}k}{\varepsilon} \tag{23}$$

With this approach the source term in the k equation, when simplified, reduces to $S_p(u_i'u_{pi}'-u_i'u_i')$, and the two terms here are of the same order of magnitude. A factor similar to the turbulent Prandtl number in single-phase flows could be chosen to represent the radial distribution of these Reynolds normal stresses. Hence Equation 22 becomes

$$S_{pk}=C_k(S_p)(\bar{u}'^2+\bar{v}'^2) \tag{24}$$

The factor C_k, however, is a flow-dependent parameter influenced by void fraction and the Reynolds number. Wang *et al.*[24] demonstrated that, for highly turbulent flows (i.e., for high liquid-flow rates and Re), the turbulence level initially decreased in the presence of the gas phase but increased with void fraction (as more gas is added). Hence C_k, which is of order unity, increases with the void fraction, α, and decreases as the Reynolds number, Re, increases. A suitable function that relates these variables is

$$C_k=\left(\frac{2.47\times10^5\alpha}{\mathrm{Re}}\right)^{2.66} \tag{25}$$

We model the bubble source term in the ε equation, using an empirical constant, C_3 (Equation 21). In choosing the value of C_3, following Parthasarathy,[39] we consider equilibrium requirements in a homogeneous stationary flow, where turbulence is generated only by bubble motion. This choice implies that $C_3\simeq C_2$ and that C_2 (1.92) is the constant in the ε equation described earlier.

The boundary conditions at the inlet are specified from known inflow conditions. Zero-normal gradient conditions prevail on the axis of symmetry for the axial velocity, U, the kinetic energy of turbulence, k, and its rate of dissipation, ε, whereas the radial velocity, V, there is zero by the virtue of symmetry. At the exit plane the conditions are not known beforehand; the assumption is that the axial gradients of all the variables vanish on this plane. For the free shear flows (i.e., the jet flows) far from the jet, the fluid has no motion. For such flows that have nonzero free-stream velocity, the simplified form of the transport equations for k and ε near the free stream, with zero gradient conditions normal to the free stream, are traditionally used. Here, the two-phase jet is in an otherwise quiescent large pool of liquid. Thus the velocities (U and V) far from the jet will be zero, and with zero velocities (and no turbulence), the turbulence parameters also vanish far from the jet.

For pipe-flow calculations in the region near the wall, the solutions are matched by the well-established wall functions,[30] where the shear stress at the wall is obtained from the log law. The shear stress at the wall, τ_w, is

$$\tau_w=\frac{\rho C_\mu^{1/4}k^{1/2}U_w\kappa}{\ln(Ey^+)} \tag{26}$$

where U_w is the liquid velocity at a distance y_w from the wall, y^+ is a dimensionless distance from the wall, $\tau_w y/\mu$, and k and E are constants; κ is Karman constant and E takes the value 9.793. The assumption of local equilibrium yields the following expression for the boundary value of ε

$$\varepsilon_w=\frac{k_w^{3/2}C_\mu^{3/4}}{\kappa y_w} \tag{27}$$

For the U and k equations, local equilibrium is used to obtain appropriate source terms, which modify their difference equations near the wall; V is assumed to vanish at the wall.

The numerical procedures used to solve Equations (1–3, 6–27) consist of calculating the continuum-phase properties, while accounting for the dispersed-phase effects in the form of source terms. We solved the continuum-phase equations using methods similar to those described by Patankar and Spalding[28] and Neti and Eichhorn.[29] Specifically, because of its superior performance,[36] we used the Van Doormal and Raithby's SIMPLEC algorithm[40] instead of the SIMPLE or SIMPLER procedures.[41] The linearized set of difference equations are solved by line-by-line iteration and a tridiagonal matrix algorithm. The equations for the dispersed phase are simple, ordinary differential equations and are solved by the Runge–Kutta method. Convergence is tested by requiring the sum of the absolute residual (difference between left- and right-hand sides of the difference equation) values to be less than 10^{-4} (1 part in 10^4) for mass and 10^{-6} for momentum. The overall solution procedure for the two-phase equations is as follows:

(1) compute a single-phase solution for the continuum phase with the turbulence model, pressure corrections, etc.;
(2) solve the bubble trajectory equations;
(3) evaluate the source term contributions of the dispersed phase that are to be included in the momentum, k, and ε equations;
(4) repeat step 1 with the newly evaluated source terms; and
(5) repeat steps 1–4 until convergence to the desired solution is obtained.

We performed the computations on a CDC Cyber 180 model 850 computer. Typical CPU time for a 36×14 grid for pipe flow (with 14 in the radial direction) with 1,600 bubbles was 1500 s. Effect of grid dependence was tested by doubling the grid, and the results were essentially the same as those presented here.

Comparison of results and discussion

The two-phase flow model and solution algorithm described were used to obtain solutions for two-phase jet and pipe flows. Computational predictions of air–water bubbly jets in still water were first tested against Sun's data.[5] The two-phase jets in question were produced by blowing air and water vertically up into a "large" tank of water through an injector of diameter

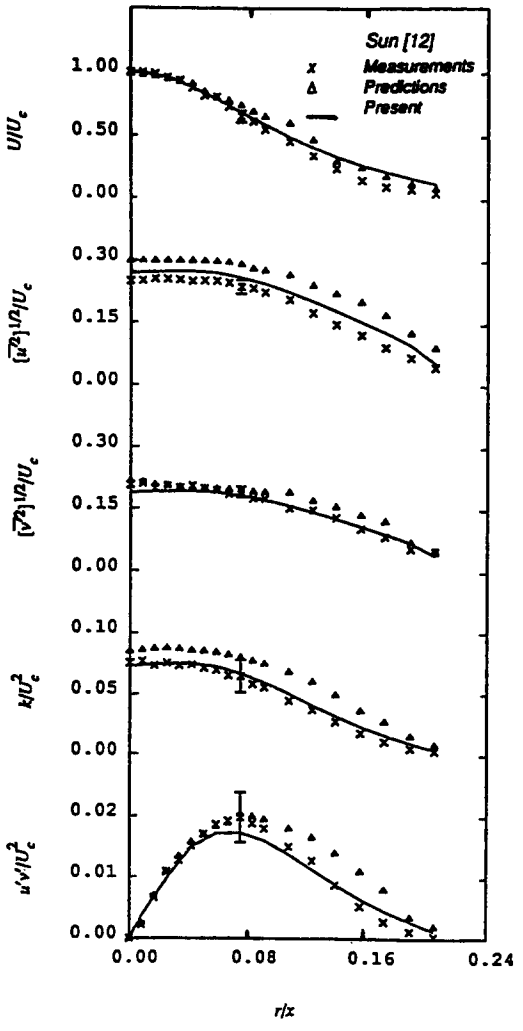

Figure 1 Radial variation of liquid-phase mean and turbulent quantities in case I two-phase jet at $x/d=24$

d. Sun *et al.*[3–5] made phase-velocity and turbulence measurements at several axial positions (x/d). We used their measurements at $x/d=8$ were used as initial conditions. The bubbly jets had different gas-volume flow-rate fractions at the jet entrance, cases I and II having values of 0.024 and 0.091, respectively. The jet radius (where the free-stream boundary conditions were specified) was determined using single-phase and two-phase bubbly jet data reported in the literature. In addition, a deterministic separated phase flow model, in which the dispersed phase interacts only with the mean properties of the continuous phase, was used for these jet predictions.

The results presented consist of the radial profiles of the mean axial velocity, the axial and radial components of fluctuating velocity, turbulence kinetic energy, and Reynolds shear stress for the continuous phase; and profiles of axial mean velocity of the dispersed phase at two axial locations ($x/d=24$ and 60, where d is the jet injector diameter) for the two gas-flow rates. Figures 1–4 illustrate the properties of the continuous phase in two-phase jets. The profiles are, of course, similar to those of single-phase jets; however, presence of the dispersed phase (bubbles) increases the turbulence levels over the single-phase jet values. The effects of buoyancy are more apparent for case II, and the turbulence kinetic energy k is some 10–30 percent larger than that of the lower void jet. In addition, k appears to increase progressively near the axis, as distance and initial gas loading increase. This feature emphasizes the need for including the bubbles' effects on continuous-phase (water) turbulence properties with flow-dependent source terms in the turbulence kinetic energy (k) and the turbulence dissipation rate (ε) equations. The levels of anisotropy of $\bar{u}'$ and $\bar{v}'$ are similar to single-phase jets at lower void fractions (case I, bubbly jet) but are larger at higher voidage.

Profiles of the bubble mean velocity at the two lower axial locations (case I) and at the largest axial location value for the higher voidage jet (case III), respectively, are shown in Figures 5 to 7. The deterministic separated flow model underestimates the radial extent of the region containing bubbles, because effects of turbulent dispersion are ignored. The predictions are terminated in the radial direction at the point of maximum bubble dispersion, because statistically there were not enough bubbles in the region where the computational results are not plotted (left blank). This lack is a deficiency in the deterministic separated phase flow model used here, because it does not account for the turbulent dispersion of the bubbles. The stochastic separated-phase flow model could have predicted such features better. Our interest here is primarily in determining the effects of dispersed phase (bubbles) on continuous-phase (liquid) properties, and the deterministic model appears to achieve that objective rather well.

Although the predicted properties of the continuous phase

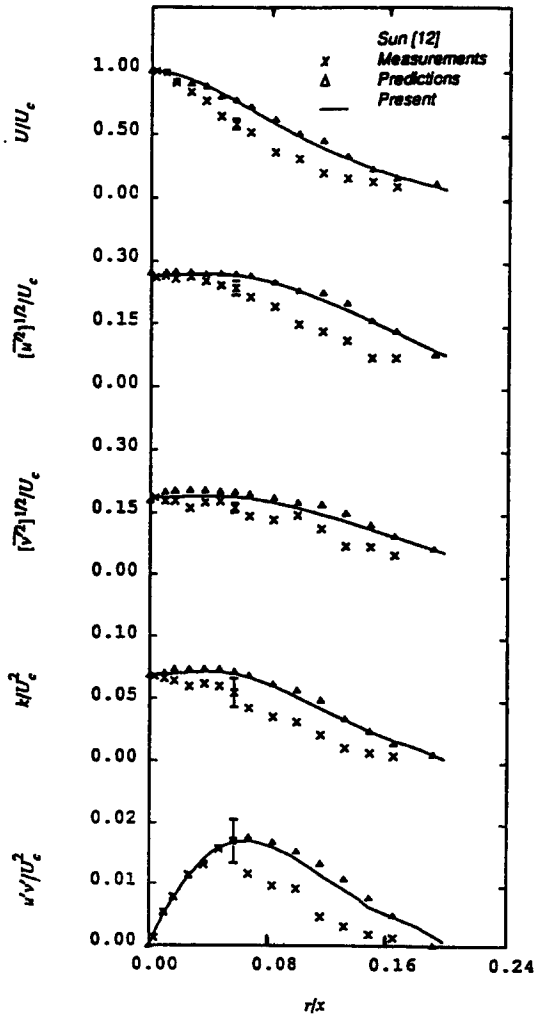

Figure 2 Radial variation of liquid-phase mean and turbulent quantities in case I two-phase jet at $x/d=60$

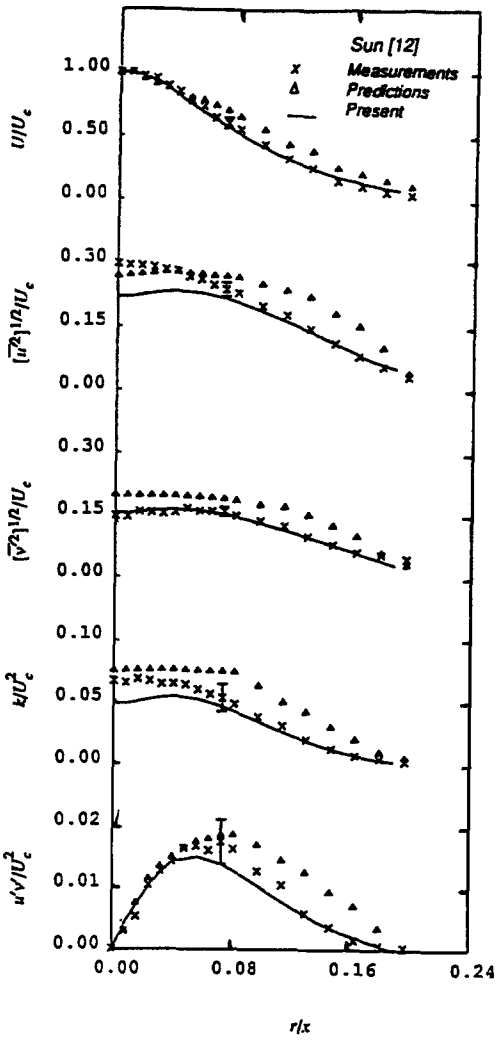

Figure 3 Radial variation of liquid-phase mean and turbulent quantities in case II two-phase jet at $x/d=24$

agree well with the measurements, there discrepancies are encountered. They may be the result of two factors: (1) the estimated initial conditions for the analysis of $x/d=8$, which in turn affects the predictions for all other axial stations; and (2) the finite width of the test tank in the experiments, which confines the flow far from the injector, as may be seen for the larger x/d values. The approach used to estimate turbulence dissipation rate, ε, is particularly problematical, because it involves several quadratic variables and evaluation of a mean velocity gradient, which lead to substantial uncertainties.

Predictions of parametric effects in two-phase pipe flows were made with a stochastic separated-phase analysis, which includes the effects of the fluctuating velocity information. Predictions of the radial variation of liquid mean axial velocity in bubbly flow are shown in Figures 8–11. As expected,[12,17,18,24] the presence of voids tends to flatten the liquid velocity profile compared to that in a single-phase pipe flow. The predicted results that are in fair agreement with the measurements do account for the increase in mixing manifested in a more uniform velocity profile. At higher Reynolds numbers (Figures 9–11), the maximum liquid velocity does not occur at the pipe centerline. For upward flows (Figures 9 and 10), the higher void concentration near the wall causes the liquid velocity to move faster because of bubble-induced drag. These trends, the so-called chimney effect, also have been reported by Theofanous and Sullivan[13] and Wang *et al.*[24] Conversely, bubble "coring" in downward flows retards the flow in the core because of buoyancy. The resultant diversion of liquid into the low-void region near the wall apparently causes the maximum liquid velocity to again occur off the centerline. The corresponding relative turbulence intensities also are presented for each of these

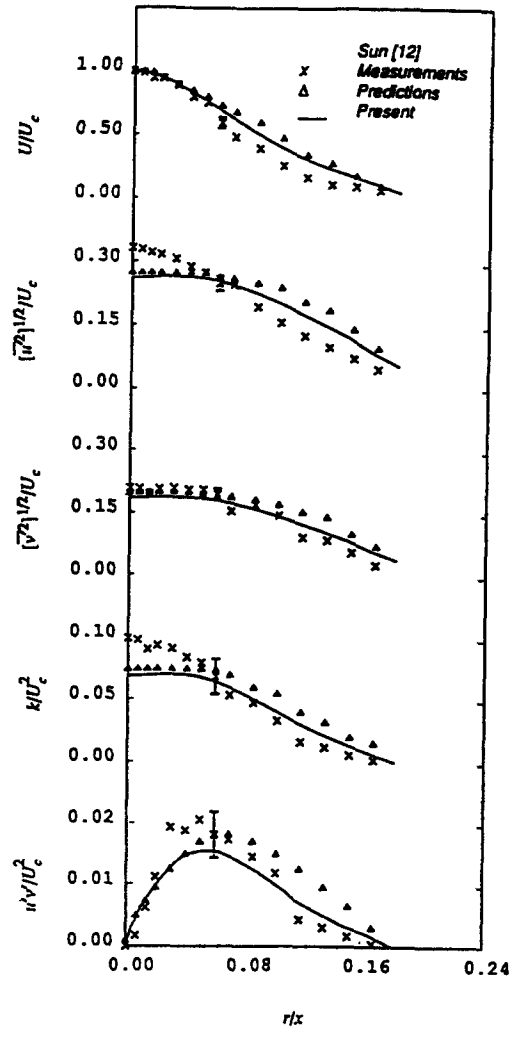

Figure 4 Radial variation of liquid-phase mean and turbulent quantities in case II two-phase jet at $x/d=60$

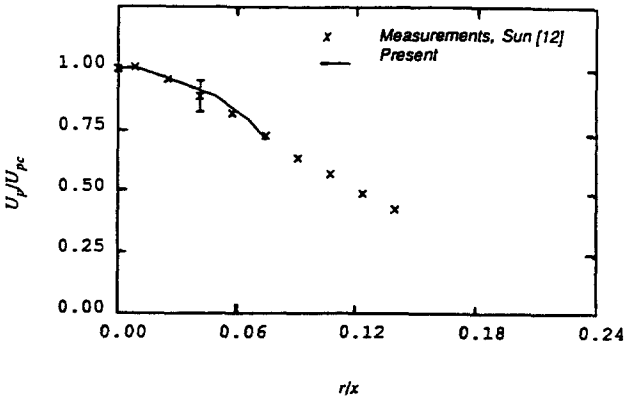

Figure 5 Radial variation of bubble-phase mean quantity in case I two-phase jet at $x/d=24$

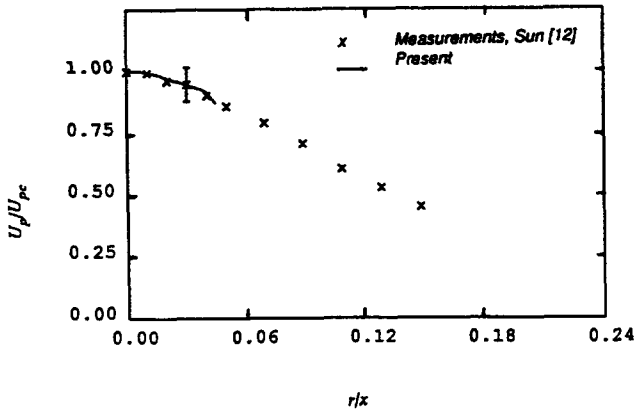

Figure 6 Radial variation of bubble-phase mean quantity in case I two-phase jet at $x/d=40$

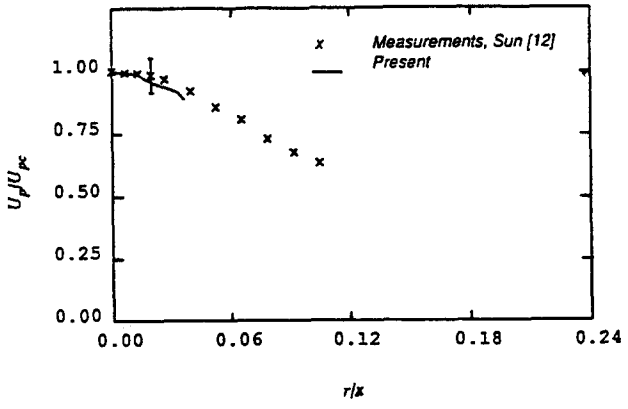

Figure 7 Radial variation of bubble-phase mean quantity in case III two-phase jet at $x/d=60$

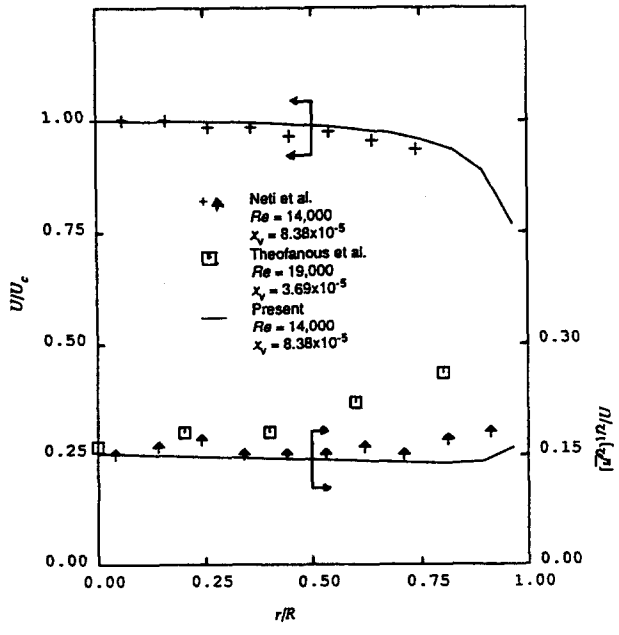

Figure 8 Radial variation of mean axial velocity and turbulent intensity, two-phase pipe flow; Re = 20,000 and $x_v = 8.38 \times 10^{-5}$

cases (Figures 8–11). Good radial mixing results in fairly uniform turbulence intensity profiles, except for the higher values (near the walls), and for downflow the turbulence intensity near the wall is not higher. The agreement between predictions and measurements in general is very good.

In the preliminary modeling of the dispersed-phase effects on continuous-phase turbulence, the constant C_k (see Equation 25) was set at 1.0 for Re = 20,000 and $\alpha = 0.08$, and reasonable agreement was achieved compared with Neti and Colella's measurements.[17] But when we used this value of C_k to model the data from Wang *et al.*[24] (Re = 35,000 and $\alpha = 0.1235$), the model overestimated the turbulence kinetic energy, k, which

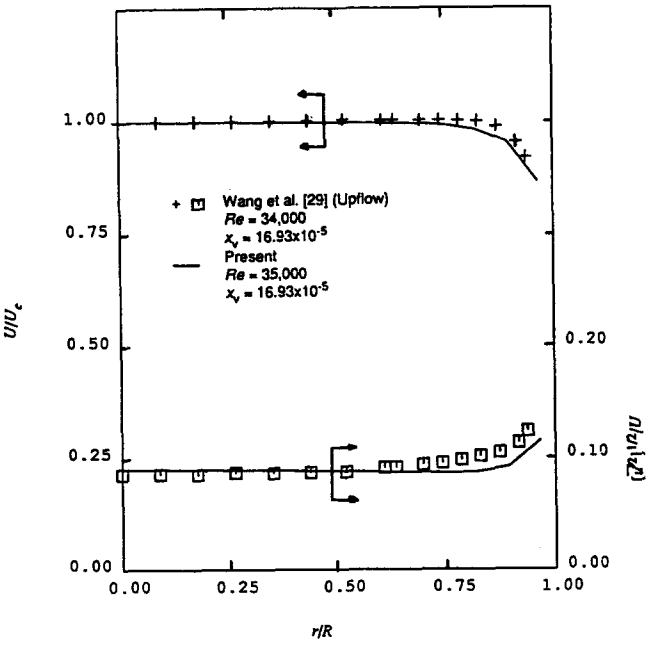

Figure 9 Radial variation of mean axial velocity and turbulent intensity, two-phase pipe upflow; Re = 35,000 and $x_v = 16.93 \times 10^{-5}$

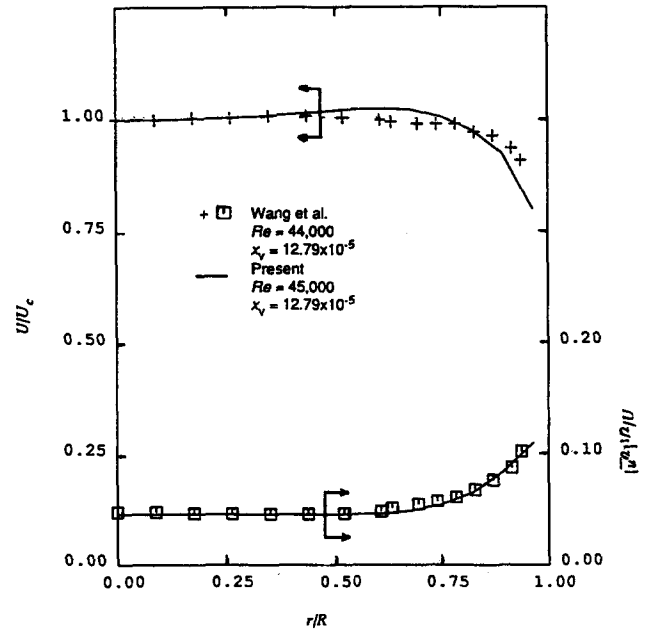

Figure 10 Radial variation of mean axial velocity and turbulent intensity, two-phase pipe upflow; Re = 45,000 and $x_v = 12.79 \times 10^{-5}$

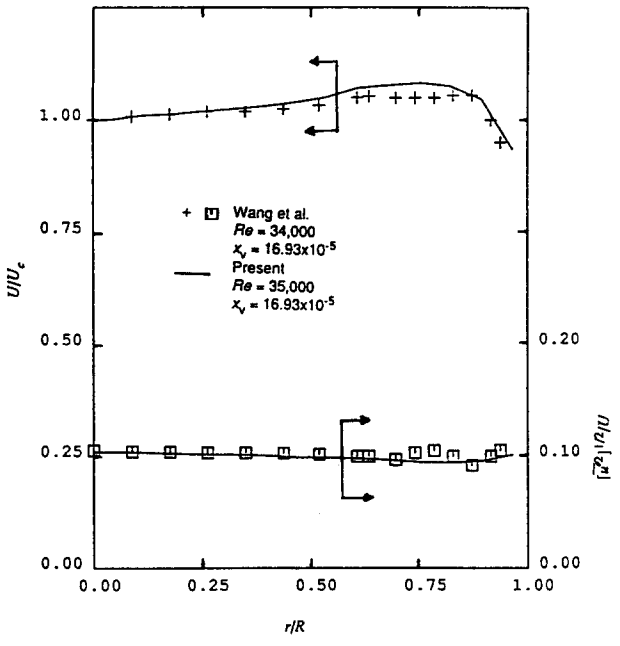

Figure 11 Radial variation of mean axial velocity and turbulent intensity, two-phase pipe downflow; Re = 35,000 and $x_v = 16.93 \times 10^{-5}$

indicated the need for a flow-dependent C_k. A linear function first proposed related C_k to Re but failed in predicting all the data. We noted that C_k must increase with the void fraction, α, and decrease as Reynolds number increases. A new function, which includes such a dependence, is

$$C_k = \left(\frac{a\alpha}{\mathrm{Re}}\right)^b \tag{28}$$

Little data is available to generalize and/or validate the relationship and to determine the new constants (a and b) in Equation 28. Nonetheless, a and b, as determined from experimental data, yield Equation 25. The relationship we used appears to work well for the conditions tested, but its generality cannot be assumed.

Normally, the turbulence level increases even for small amounts of dispersed phase introduced into the liquid phase.[5,12,13,17,18,24] Figure 12 shows that, for our results, an increase in quality implies an increase in mainstream turbulence for upflow, which indicates increased mixing. This increased mixing is associated with increased momentum transfer and hence more and more uniform velocity profiles, as shown. As expected, the relative turbulence intensity increases near the wall, and the effect of quality diminishes as the wall shear controlled turbulence region is approached.

Conclusions

The mathematical models describing two-phase bubbly flows derived from the fundamental Navier–Stokes equations and their numerical solutions have been described and discussed. The following are the major observations and conclusions of this study.

(1) Finite difference computations in two-phase flow, using an Eulerian system to describe the continuous phase (water) and a Lagrangian approach for the dispersed phase (bubbles) can be coupled by means of the source terms concept.

(2) A deterministic separated phase flow model was used to predict the two-phase bubbly jet flows and a stochastic separated-phase model was used in tracking the bubbles in circular-pipe, two-phase bubbly flows. The bubble movements are a function of the liquid mean velocities in the deterministic model, whereas fluctuating velocity information also is used by the stochastic model.

(3) The presence of bubbles in the flow increased the turbulence in the inner (core) region and enhanced wall-generated turbulence as well. An additional constant in the k equation, C_k, dependent on flow Reynolds number and void fraction, had to be introduced to predict existing experimental data. An order of magnitude analysis was used to evaluate the effect of bubbles and the empirical constant in the ε equation.

(4) Predictions of the two-phase jet flow agreed well with experiments for all the parameters except bubble dispersion. We believe that this result comes from using the deterministic model, which does not account for the effect of the fluctuating velocities.

(5) Turbulence production near the wall in pipe flow—caused by presence of the second phase—was accounted for by modifying the mixing layer as a function of two-phase quality, and the two-phase near wall function is thus correspondingly a modified form of the single-phase wall function.

(6) In pipe flows the presence of voids tends to flatten the axial liquid velocity profiles compared to those in single-phase flows. The computed results, which are in good agreement with the measurements, predicted the increase in mixing and the more uniform axial velocity profiles. Except at very low Reynolds numbers, the maximum liquid velocity occurred at a radial location close to the wall and not at the pipe centerline.

(7) Turbulence levels of the continuous phase in the two-phase flow increased with void fraction. But, for a given void fraction, the effect of the dispersed phase on the turbulence levels appears to be smaller at higher Reynolds numbers.

Summary

A two-equation turbulent model for steady incompressible two-phase flows was developed to predict bubbly noncon-

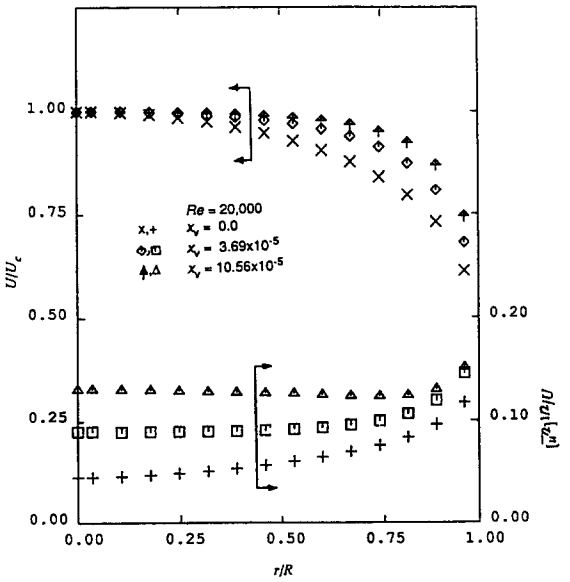

Figure 12 Computed radial variation of axial mean velocity and turbulent intensity; effect of vapor quality, two-phase bubble pipe flow; Re = 20,000

densing jet and pipe flows from the Navier–Stokes equations. The numerical computations used an Eulerian system to describe the continuous (liquid) phase and a Lagrangian approach for simulating the effects of the dispersed (gaseous) phase. The addition of even small amounts of gas to the flow increased turbulence levels noticeably. At higher void fractions, the effects of the second phase were large, and the need for a detailed modeling of the turbulent energy production and dissipation mechanisms to describe the flow is justified. The flow computations yielded good predictions for the radial distributions of mean velocity, and turbulence intensity.

References

1 Ishii, M. and Mishima, K. Two-fluid model and hydrodynamic constitutive relations. *Nucl. Eng. Des.*, 1984, **82**(2&3), 107–126

2 Sun, T-Y. and Faeth, G. M. Structure of turbulent bubbly jets, I: Methods and centerline properties. *Int. J. Multiphase Flow*, 1986, **12**(1), 99–114

3 Sun, T-Y. and Faeth, G. M. Structure of turbulent bubbly jets, II: Phase property profiles. *Int. J. Multiphase Flow*, 1986, **12**(1), 115–126

4 Sun, T-Y., Parthasarathy, R., and Faeth, G. M. Structure of bubbly round condensing jets. *J. of Heat Transfer*, 1986, **108**, 951–959

5 Sun, T-Y. A theoretical and experimental study of noncondensing turbulent bubbly jets. Ph.D. dissertation, The Pennsylvania State University, University Park, PA, 1985

6 Schor, A. L., Kazimi, M. S., and Todreas, N. E. Advances in two-phase flow modeling for LMFBR applications. *Nucl. Eng. Des.*, 1984, **82**(2&3), 127–155

7 Spore, J. W. *et al.* TRAC-BD1: An advanced best estimate computer program for boiling water reactor loss-of-coolant accident analysis. NUREG/CR-2178, October 1981

8 Abdel-Aal, H. K., Stiles, G. B., and Holland, C. D. Formation of interfacial area at high rates of gas flow through submerged orifices. *AIChE J.*, 1966, **12**, 174–180

9 Goldschmidt, V. W., Householder, M. K., Ahmadi, G., and Chuang, S. C. Turbulent diffusion of small particles suspended in turbulent jets. *Prog. in Heat and Mass Transfer*, 1971, **6**, 487–508

10 Chesters, A. K., Van Doorn, M., and Goossens, L. H. J. A general model for unconfined bubble plumes from extended sources. *Int. J. Multiphase Flow*, 1980, **6**, 499–521

11 Shuen, J-S., A theoretical and experimental investigation of dilute particle-laden turbulent gas-jets. Ph.D. dissertation, The Pennsylvania State University, State College, PA, 1983

12 Theofanous, T. G. and Sullivan, J. The use of LDA in two-phase bubble pipe flow. *Proc. Third International Workshop on Laser Velocimetry*, West Lafeyatte, IN, Hemisphere, 1979, 391–394

13 Theofanous, T. G. and Sullivan, J. Turbulence in two-phase dispersed flows. *J. Fluid Mech.*, 1982, **116**, 343–362

14 Serizawa, A., Katuoka, I., and Michiyoshi, I. Turbulence structure of air-water bubbly flow: Measuring techniques. *Int. J. Multiphase Flow*, 1975, **2**, 221–233

15 Serizawa, A., Katuoka, I., and Michiyoshi, I. Turbulence structure of air-water bubbly flow, II: Local properties. *Int. J. Multiphase Flow*, 1975, **2**, 235–246

16 Serizawa, A., Katuoka, I., and Michiyoshi, I. Turbulence structure of air-water bubbly flow, III: Transport properties. *Int. J. Multiphase Flow*, 1975, **2**, 247–259

17 Neti, S. and Colella, G. Development of a fiber-optic Doppler anemometer for bubbly two-phase flows. EPRI Report 1159-3, 1983

18 Marie, J. L. Investigation of two-phase bubbly flows using laser Doppler anemometry. *Physiochem. Hydro.*, 1983, **4**(2), 103–118

19 Lance, M. and Bataille, J. Turbulence in the liquid phase of bubbly air-water flow. Paper presented at NATO Workshop, Schliersee, FRG, 1982

20 Bankoff, S. G. A variable density single-fluid model for two-phase flow with particular reference to steam-water flow. *J. Heat Transfer*, 1960, **80**(2), 265–270

21 Levy, S. Prediction of two-phase pressure drop and density distribution from mixing length theory. *J. Heat Transfer*, 1963, **85**(2), 137–152

22 Beattie, D. R. H. Two-phase flow structure and mixing length theory. *J. Nucl. Eng. Des.*, 1972, **21**, 46–64

23 Sekoguchi, K., Kawakami, Y., and Nishikawa, L. Flow simulation of forced flow boiling with air-water two-phase fluids. *Bull. JMSE*, 1976, **19**(128), 187–194

24 Wang, S. K., Lee, S. J., Jones, O. C., and Lahey, R. T. 3-D turbulence and phase distribution in bubbly two-phase flows. *Int. J. Multiphase Flow*, 1987, **13**(3), 327–343

25 Spindler, K., Bierer, M., Lorenz, G., Erhard, A., and Hahne, E. Measurements in vertical gas liquid two-phase flows using an optical fibre probe. Paper presented at First World Conf. on Exp. Heat Transfer, Fluid Mech. and Thermo., Dubrovnik, Yugoslavia, Sept. 4–9, 1988

26 Herringe, R. A. and David, M. R. Structural development of gas-liquid mixture flows. *J. Fluid Mech.*, 1973, **73**, 97–123

27 Herringe, R. A. and Davis, M. R. Flow structure and distribution effects in gas-liquid mixture flows. *Int. J. Multiphase Flow*, 1978, **4**, 461–486

28 Patankar, S. V. and Spalding, D. B. A calculation procedure for heat, mass and momentum transfer in three-dimensional parabolic flows. *Int. J. Heat and Mass Transfer*, 1972, **15**, 1787

29 Neti, S. and Eichhorn, R. Computation of developing turbulent flow in a square duct. *Turbulent Boundary Layers* (H. E. Weber *et al.*, Eds.), ASME Book No. G00145, 1978

30 Launder, B. E. and Spalding, D. B. *Mathematical Models of Turbulence*, Academic Press, New York, 1972

31 Soo, S. L. *Fluid Dynamics of Multiphase Systems*, Blaisdell, Waltham, MA, 1967

32 Wallis, G. B. *One-Dimensional Two-Phase Flow*, McGraw-Hill, New York, 1969

33 Clift, R., Grace, J. R., and Weber, M. E. *Bubbles, Drops and Particles*, Academic Press, New York, 1978

34 Peebles, F. N. and Garber, H. J. Studies on the motion of gas bubbles in liquids. *Chem. Eng. Prog.*, 1953, **49**(2), 88–97

35 Shuen, J. S., Chen, L. D., and Faeth, G. M. Prediction of the structure of turbulent, particle-laden round jets. *AIAA J.*, 1983, **21**(1), 1438

36 Mohamed, O. E. E. Prediction of turbulent two phase bubbly flows in vertical pipes, Ph.D. dissertation, Lehigh University, Bethlehem, PA, 1988

37 Al-Taweel, A. M. and Landau, J. Turbulence modulation in two-phase jets. *Int. J. Multiphase Flow*, 1977, **3**, 341–351

38 Shuen, J. S., Chen, L. D., and Faeth, G. M. Evaluation of a stochastic model of particle dispersion in a turbulent round jet. *AIChE J.*, 1983, **29**(1), 167

39 Parthasarathy, R. N. and Faeth, G. M. Structure of particle-laden turbulent water jets in still water. *Int. J. Multiphase Flow*, 1987, **13**(5), 699–716

40 Van Doormaal, J. P. and Raithby, G. D. Enhancements of the SIMPLE method for predicting incompressible fluid flows. *Num. Heat Transfer*, 1984, **7**, 147–163

41 Patankar, S. V. *Numerical Heat Transfer and Fluid Flow*, McGraw-Hill, New York, 1980